2013–2019 increases of surface ozone pollution in China: anthropogenic and meteorological influences

Ke Li[1], Daniel J. Jacob[1], Lu Shen[1], Xiao Lu[1], Isabelle De Smedt[2], and Hong Liao[3,4]

[1]John A. Paulson School of Engineering and Applied Sciences, Harvard University, Cambridge, MA, USA
[2]Belgian Institute for Space Aeronomy (BIRA-IASB), Brussels, Belgium
[3]Jiangsu Key Laboratory of Atmospheric Environment Monitoring and Pollution Control, Collaborative Innovation Center of Atmospheric Environment and Equipment Technology, School of Environmental Science and Engineering, Nanjing University of Information Science and Technology, Nanjing, China
[4]Harvard-NUIST Joint Laboratory for Air Quality and Climate, Nanjing University of Information Science and Technology, Nanjing, China

Correspondence to: Ke Li (keli@seas.harvard.edu)

Abstract. Surface ozone data from the Chinese Ministry of Ecology and Environment (MEE) network show sustained increases across the country over the 2013–2019 period. Despite Phase 2 of Clean Air Action targeting ozone pollution, ozone was higher in 2018–2019 than in previous years. The mean summer 2013–2019 trend of maximum 8-h average (MDA8) ozone was 1.9 ppb a^{-1} ($p<0.01$) across China and 3.3 ppb a^{-1} ($p<0.01$) in the North China Plain (NCP). Fitting ozone to meteorological variables with a multiple linear regression model shows that meteorology played a significant but not dominant role in the 2013–2019 ozone trend, contributing 0.70 ppb a^{-1} ($p<0.01$) across China and 1.4 ppb a^{-1} ($p=0.02$) in the NCP. Rising June-July temperatures over the NCP were the main meteorological driver, particularly in recent years (2017–2019), and were associated with increased foehn winds. NCP data for 2017–2019 show a 15% decrease in fine particulate matter ($PM_{2.5}$) that may be driving the continued anthropogenic increase in ozone, and flat emissions of volatile organic compounds (VOCs). VOC emission reductions, as targeted by Phase 2 of the Chinese Clean Air Action, are needed to reverse the increase of ozone.

1 Introduction

Surface ozone is a serious air pollution issue over much of eastern China (Ma et al., 2012; Fu et al., 2019). Measurements from the Chinese Ministry of Environment and Ecology (MEE) network of sites frequently exceed the national air quality standard of 160 μg m^{-3}, corresponding to 82 ppb at 298 K and 1013 hPa (Li et al., 2017; Shen et al., 2019a; Fan et al., 2020). The Clean Air Action initiated in 2013 imposed rapid decreases in pollutant emissions (Chinese State Council, 2013) and resulted in large decreases in fine particulate matter ($PM_{2.5}$) concentrations (Zhai et al., 2019; Q. Zhang et al., 2019). However, ozone increased by 1–3 ppb a^{-1} over the 2013–2017 period in megacity clusters of eastern China (Lu et al., 2018; Li et al., 2019a; Lu et al. 2020), partly offsetting the health benefits from improved $PM_{2.5}$ (Dang and Liao, 2019; Q. Zhang et al., 2019). Phase 2 of Clean Air Action starting in 2018 (Chinese State Council, 2018) imposed new emission controls targeted at ozone. Here we show that the increasing ozone trend in eastern China has continued through 2019, driven by both anthropogenic emission and meteorological trends, and stressing the urgent need for more vigorous emission controls.

Ozone in polluted regions is produced by photochemical reactions of volatile organic compounds (VOCs) and nitrogen oxides ($NO_x \equiv NO + NO_2$), enabled by hydrogen oxide radicals ($HO_x \equiv OH$ + peroxy radicals) as oxidants. VOCs and NO_x are emitted by fuel combustion, and VOCs have additional industrial sources (Zheng et al., 2018) and biogenic sources (Guenther et al., 2012). HO_x is produced photochemically from ozone and water, formaldehyde (HCHO), nitrous acid, and other precursors (Tan et al., 2019). Ozone is highest in summer when photochemistry is most active (Wang et al., 2017). Meteorological conditions play an important role in modulating ozone concentrations, not only through transport but also by affecting natural emissions and chemical rates (Jacob and Winner, 2009; Shen et al., 2016; Fu et al., 2019; Lu et al., 2019).

A number of studies have investigated the roles of anthropogenic and meteorological factors in driving the 2013–2017 ozone trend, and concluded that meteorological factors were not negligible but anthropogenic factors were dominant (Ding et al., 2019; Li et al., 2019a; Liu et al., 2019; Yu et al., 2019; Liu et al., 2020). Our previous work (Li et al., 2019a, 2019b) found that the decrease of $PM_{2.5}$ was a major factor driving the increase of ozone due to the role of $PM_{2.5}$ as scavenger of hydroperoxy (HO_2) radicals and NO_x that would otherwise produce ozone. Here we extend the analysis of ozone trends to 2019, into the implementation of Clean Air Action Phase 2, and bring in satellite and ground-based observations to relate the most recent ozone trends to those of VOC (Shen et al., 2019b) and NO_x emissions (Zheng et al., 2018; Shah et al., 2020).

2 Data and methods

2.1 Surface measurements

Hourly concentrations of ozone, $PM_{2.5}$, and NO_2 are taken from the MEE website (http://106.37.208.233:20035) and archived at http://beijingair.sinaapp.com. The network was launched in 2013 as part of the Clean Air Action. It included 450 monitoring stations in 2013, growing to ~1500 stations by 2019. We compute maximum daily 8-h average (MDA8) ozone as well as 24-h average $PM_{2.5}$ and NO_2 concentrations from the hourly data for June-July-August (JJA). Concentrations were reported by the MEE in units of μg m^{-3} under standard conditions (273 K, 1013 hPa) until 31 August 2018. This reference state was changed on 1 September 2018 to (298 K, 1013 hPa) for gases and local ambient state for $PM_{2.5}$ (MEE, 2018). We converted ozone and NO_2 concentrations to ppb, and rescaled post-August 2018 $PM_{2.5}$ concentrations to standard conditions by assuming (298 K, 1013 hPa) as the local ambient state.

2.2 Satellite observations

We use observations of NO_2 and formaldehyde (HCHO) columns from the OMI and TROPOMI satellite instruments to track recent changes in anthropogenic emissions of NO_x and VOCs, respectively. Shen et al. (2019b) and Shah et al. (2020) previously found that OMI-derived trends of VOC and NOx emissions were consistent with 2013–2017 bottom-up estimates from the Multi-resolution Emission Inventory for China (MEIC; Zheng et al., 2018). Here we extend the analysis using 2013–2019 OMI data from the European Quality Assurance for Essential Climate Variables project for NO_2 (Boersma et al., 2018) and HCHO (De Smedt et al., 2015). We further use TROPOMI HCHO data available for the summers of 2018–2019 for (De Smedt et al., 2018). We do not use TROPOMI NO_2 data because of a version change in March 2019 from v1.2.0 to v1.3.0 that could bias the trend between the summers of 2018 and 2019 (https://sentinel.esa.int/documents/247904/2474726/Sentinel-5P-Level-2-Product-UserManual-Nitrogen-Dioxide, last access: 20 July 2020). The TROPOMI HCHO data are freely accessed from https://s5phub.copernicus.eu/dhus/ (last access: 28 February 2020) and we only use observations with quality assurance value larger than 0.5. This filter effectively removes data with cloud fraction larger than 0.5. Interannual trends in HCHO columns could be affected by temperature-dependent emissions of biogenic VOCs (Palmer et al., 2006). Following Zhu et al. (2017), we remove this contribution by regressing JJA monthly mean HCHO columns onto noon (13:00 local time) surface air temperatures, and then subtracting this fitted temperature dependency.

2.3 Stepwise multiple linear regression (MLR) model

To quantify the role of meteorology in driving 2013–2019 ozone trends, we use the same stepwise multiple linear regression (MLR) modeling approach as Li et al. (2019a). This modeling approach relates the month-to-month variability

of MDA8 ozone to that of meteorological variables. Consistent meteorological fields for 2013–2019 were obtained from the NASA Modern-Era Retrospective Analysis for Research and Applications, Version 2 (MERRA-2) product (https://gmao.gsfc.nasa.gov/reanalysis/MERRA-2, last access: 28 February 2020) (Gelaro et al., 2017). The MERRA-2 data have a spatial resolution of 0.5° latitude × 0.625° longitude. We average the daily MDA8 ozone from the MEE network onto the MERRA-2 grid. Firstly, the regression model is applied to select the key meteorological parameters driving the day-to-day variability of ozone for each grid cell. There are nine MERRA-2 meteorological variables considered as ozone covariates, including daily maximum 2-m air temperature (Tmax), 10-m zonal wind (U10) and meridional wind (V10), boundary layer height (PBLH), total cloud area fraction (TCC), rainfall (Rain), sea level pressure (SLP), relative humidity (RH), and 850-hPa meridional wind (V850), following (Li et al., 2019a). The meteorology fields are averaged over 24 h for use in the MLR model except for PBLH and TCC, which are averaged over daytime hours (8–20 local time), and for Tmax (daily maximum).

Secondly, to avoid overfitting, only the three locally dominant meteorological parameters are regressed onto the deseasonalized monthly MDA8 ozone to fit the role of 2013–2019 meteorological variability. The top three variables are selected based on their individual contribution to the regressed ozone, along with the requirement that they are statistically significant above the 95% confidence level in the MLR model. They will differ for each 0.5° × 0.625° grid cell. We show these top three meteorological drivers for ozone variability in Figure S1–S3 for different locations in China.

Thirdly, we fit the observed monthly ozone anomalies by applying these dominant meteorological drivers in the MLR model. The coefficients of determination (R^2) for the MLR model are generally above 0.4–0.5 for polluted regions of China which are of most interest to us (Figure S4). Remote locations with background ozone levels have less ozone variability and are thus harder to fit. Similar MLR models have been extensively employed to quantify the effect of meteorological variability on air pollutants (e.g., Tai et al., 2010; Otero et al., 2018; Zhai et al., 2019; Han et al., 2020).

Finally, the trend in regressed ozone is taken to reflect the meteorological contribution, and the residual is then taken to reflect the presumed anthropogenic contribution, with the statistical significance of the anthropogenic trend determined by Student's *t*-test. We have followed this approach before to isolate the anthropogenic trends of ozone and $PM_{2.5}$ (Li et al., 2019a; Zhai et al., 2019). Similar statistical decomposition of anthropogenic and meteorological contributions to air pollutant trends has been also employed by previous studies (e.g., Chen et al. 2019; Yu et al., 2019; X. Zhang et al., 2019). The effect of biogenic VOCs on ozone trends depends on meteorological and land cover drivers. Meteorological drivers, in particular temperature, would be accounted for in the MLR model. The effect of land cover changes is expected to be small over the 7-year time horizon of our analysis (Fu and Tai, 2014)

3 Results and discussion

We first present the general 2013–2019 summer ozone trends in China and their statistically decomposed meteorological and anthropogenic contributions. Ozone trends over the major megacity clusters in China are highlighted. We go on to more specifically attribute the meteorological and anthropogenic drivers of recent ozone trends over the North China Plain, where the ozone increase is the highest.

3.1 2013–2019 ozone trends: anthropogenic and meteorological contributions

Figure 1 shows 2013–2019 trends of summer maximum and mean MDA8 ozone and $PM_{2.5}$ from the MEE network. The Clean Air Action has dramatically improved $PM_{2.5}$ pollution since 2013, with ~50% decrease of mean summertime mean $PM_{2.5}$ concentrations across eastern China over the 2013–2019 period. Maximum $PM_{2.5}$ concentrations experienced a similar decrease trend. In contrast, ozone has been steadily increasing over 2013–2019 and concentrations in 2019 are the highest in the record. The Clean Air Action focused specific attention on the four megacity clusters identified by rectangles: North China Plain (NCP; 34°–41°N, 113°–119°E), Yangtze River Delta (YRD, 30°–33°N, 119°–122°E), Pearl River Delta (PRD, 21.5°–24°N, 112°–115.5°E), and Sichuan Basin (SCB, 28.5°–31.5°N, 103.5°–107°E). Mean MDA8 ozone in summer 2019 averaged 83 ppb across the NCP sites and maximum MDA8 ozone averaged 129 ppb. Summer mean MDA8 ozone in 2019 was lower for the other megacity clusters (67 ppb for YRD, 46 ppb for PRD, and 57 ppb for SCB) but summer maximum MDA8 ozone values were comparable to the NCP. These three megacity clusters are subject to similar ozone pollution episodes under stagnant conditions as the NCP (Wang et al., 2017), but they are more frequently ventilated by the summer monsoon bringing cleaner tropical air and precipitation hence the lower mean ozone.

Figure 2a shows the 2013–2019 trends in summer mean MDA8 ozone obtained by ordinary linear regression of the data averaged over the 0.5° × 0.625° MERRA-2 grid. Ozone increases almost everywhere in China. Decreases are largely restricted to the Shandong Peninsula and northeastern China (including Heilongjiang, Jilin, and Liaoning provinces). The mean trend for China is 1.9 ppb a^{-1} ($p<0.01$). Trends in the four megacity clusters are 3.3 ppb a^{-1} ($p<0.01$) for NCP, 1.6 ppb a^{-1} ($p<0.01$) for YRD, 1.1 ppb a^{-1} ($p=0.03$) for PRD, and 0.7 ppb a^{-1} ($p=0.23$) for SCB (Table 1). The increases are largest in the NCP, which could be explained by greater influence of radical scavenging by $PM_{2.5}$ (Li et al., 2019a, 2019b).

Figure 2b shows the meteorologically driven ozone trends, as determined by fitting ozone to meteorological variables with the MLR model. We find an average meteorologically driven trend of 0.7 ppb a^{-1} ($p<0.01$) for China. Ozone trends over 2013–2019 in the NCP and PRD are significantly contributed by meteorology, and this is particularly driven by 2018–2019 (Table 1). Similar to our previous study for 2013–2017 (Li et al., 2019a), the most important meteorological

predictor variables in the MLR model are daily maximum temperature for the NCP and meridional wind at 850 hPa for the PRD (Figure S1). These dominant meteorological parameters are also consistent with the findings from other studies (Gong and Liao, 2019; Wang et al., 2019; Han et al., 2020). Hot weather is the main meteorological driver for high ozone in the NCP, and we will elaborate on this in the next section. The main meteorological driver for the ozone increase in the PRD is the weakening of the summer monsoonal flow (**Figure 3**) that ventilates the PRD with marine air.

On the other hand, we find that meteorology mitigated ozone pollution increases over northeastern China and the Shandong Peninsula. As shown in Figure S2, summer ozone in the Shandong Peninsula is strongly affected by maritime inflow (J. Zhang et al, 2019; Han et al., 2020) which increased over the 2013–2019 period (**Figure 3**). Temperature decreased over northeastern China (**Figure 3**).

Removing the meteorological contribution in the ozone trend leaves a residual trend that we interpret as anthropogenic (**Figure 2c**), following Li et al. (2019a) and Zhai et al. (2019). This anthropogenic trend is more uniformly positive at a national scale than the observed and meteorologically driven trends. It averages 1.2 ppb a^{-1} ($p<0.01$) for all of China, as compared to 0.7 ppb a^{-1} ($p<0.01$) for the meteorologically driven trend. The observed 2013–2019 ozone increase in all the megacity clusters except the PRD is dominated by the anthropogenic contribution, averaging 1.9 ppb a^{-1} ($p<0.01$) for the NCP. This result still stands if only continuous records since 2013 are used in the analysis (Figure S5). The ozone increase in PRD is mainly meteorologically driven due to reduced monsoonal winds (**Figure 3**). The following sections present further analysis of the 2013–2019 ozone trend in the NCP, where both meteorological and anthropogenic contributions are particularly large.

3.2 Meteorologically driven 2013–2019 ozone increase in the North China Plain

Separating the observed 2013–2019 ozone trends by month shows that the seasonal JJA trend of 3.3 ppb a^{-1} ($p<0.01$) over the NCP is driven by June and July. Observed trends are 5.5 ppb a^{-1} ($p<0.01$) for June, 3.7 ppb a^{-1} ($p<0.01$) for July, and 0.9 ppb a^{-1} ($p=0.34$) for August. This month-to-month difference is mainly driven by meteorology. As derived from the MLR model, the meteorologically driven ozone trend of 1.4 ppb a^{-1} ($p=0.02$) for JJA breaks down to 3.1 ppb a^{-1} ($p<0.01$) for June, 2.2 ppb a^{-1} ($p=0.08$) for July, and –1.0 ppb a^{-1} ($p=0.16$) for August. The residual anthropogenic trend is much more similar across months (2.4 ppb a^{-1} ($p=0.02$) in June, 1.5 ppb a^{-1} ($p=0.07$) in July, 1.9 ppb a^{-1} ($p<0.01$) in August), as would be expected after removing meteorological influence.

Figure 4 shows the monthly mean time series of daily maximum temperature averaged over the NCP for 1980–2019, with 2013–2019 highlighted in shading. Temperature is the principal driver of the meteorologically driven ozone trend as indicated by the MLR model. We find a large 2013–2019 increase in temperature in June (0.42 °C a^{-1}), a lesser increase

in July (0.22 °C a^{-1}), and a decrease in August (–0.18 °C a^{-1}), reflected in the meteorologically driven ozone trend for each month. When placed in the context of the 1980–2019 record, we see that the 2013–2019 temperature trends reflect interannual climate variability rather than a long-term warming trend.

Hot weather in the NCP in the summer is generally driven by large-scale anticyclonic conditions, and this has been viewed as the principal predictor of ozone pollution days (Gong and Liao, 2019). Foehn wind conditions featuring warm and dry air subsiding from the mountains that are to the north and west of the NCP (Chen and Lu, 2016) also lead to high ozone pollution in the NCP. Foehn winds are most important in June. Following Chen and Lu (2016), we diagnosed foehn conditions in the NCP with a foehn index defined by the 850 hPa northwesterly wind averaged along a section from (42°N, 108°E) to (38°N, 112°E) (**Figure 5**). The days with positive (negative) foehn index are taken as foehn (no-foehn) condition. We find that foehn conditions are largely responsible for the 2013–2019 increase in temperature in June (**Figure 5**). The frequency of foehn conditions under hot days in June increased by 85% over the 2013–2019 period (driven mainly by the increased frequency in 2018–2019), and ozone increase under foehn conditions is 1.2 ppb a^{-1} larger than under no-foehn conditions. Our result highlights the previously unrecognized effect of foehn winds on ozone pollution in the NCP.

3.3 Anthropogenically driven 2013–2019 ozone increase in the North China Plain

Figure 6a shows the observed time series of monthly mean JJA MDA8 ozone anomalies for 2013–2019 relative to the JJA 2013–2019 mean, averaged over all MEE sites in the NCP and including sites with partial records. We see large month-to-month variability superimposed on the long-term trend. Much of this month-to-month variability can be attributed to meteorological factors using the MLR model (blue line), as discussed in the previous section. The residual anthropogenic trend (red line) shows a 2013–2019 increasing trend with much less month-to-month variability than the original observed time series. The standard deviation decreases from 8.8 ppb to 5.3 ppb after removal of meteorological influence.

Figure 6b shows the 2013–2019 observed trends of different quantities relevant to the anthropogenic ozone trend over the NCP: $PM_{2.5}$ and NO_2 from the MEE network, and NO_2 and HCHO tropospheric columns from satellites. $PM_{2.5}$ shows a steady decrease, 49% over the 2013–2019 period. NO_2 (a proxy for NO_x emissions; Zheng et al., 2018) shows a 25–30% decrease with some interannual variability that is consistent between the OMI satellite data and the surface MEE network. HCHO (a proxy for VOC emissions) shows no significant trend for the 2013–2019 period, with some interannual variability that could reflect noise in the measurement (Shen et al., 2019b).

Of particular interest are the trends for 2017–2019, extending beyond the currently available MEIC emission inventory (Zheng et al., 2018) and during which we find continued increase of ozone. Relative to 2017, we find for 2019 a 15% decrease in $PM_{2.5}$, a 6–10% decrease in NO_x emissions (depending on which proxy record we use), and flat VOC emissions. Phase 2 of the Chinese government's Clean Air Action (China State Council, 2018) called for a 18% decrease in $PM_{2.5}$ over 2015–2020, a 15% decrease in NO_x emissions, and a 10% decrease in VOC emissions. Taking into account the already-achieved 2015–2017 gains in $PM_{2.5}$ and NO_x emissions, Li et al. (2019b) inferred that those targets would require 2017–2020 decreases of 8% for $PM_{2.5}$, 9% for NO_x emissions, and 10% for VOCs emissions. They found from model simulations that the decrease in $PM_{2.5}$ would cause further increase in ozone, but that decreasing VOC emissions would compensate and enable net improvement, with NO_x emission changes having relatively little effect. We find here that the observed 2017–2019 decrease in $PM_{2.5}$ goes beyond the Clean Air Action target, while the satellite HCHO data show no evidence of a decrease in VOC emissions. Combination of these two effects is consistent with the observed anthropogenically driven increase in ozone over 2017–2019. Decrease of VOC emissions is the key to reverse the ozone increase (Li et al., 2019b).

4 Conclusions

Surface ozone data from the Chinese Ministry of Environment and Ecology (MEE) network show a sustained nationwide increase over the 2013–2019 period, with a few exceptions (Shandong Province and northeastern China), and with particularly high concentrations in 2018–2019. Correction for meteorologically driven trends with a multiple linear regression (MLR) model shows a general pattern of anthropogenically driven ozone increase across China, though meteorological influences are also significant. The mean summer (JJA) 2013–2019 increase in maximum daily 8-hour average (MDA8) ozone over China is 1.9 ppb a^{-1} ($p<0.01$), including 0.7 ppb a^{-1} ($p<0.01$) from meteorologically driven trends (mostly temperature and circulation) and 1.2 ppb a^{-1} ($p<0.01$) from anthropogenic influence. Ozone concentrations are highest in the North China Plain (NCP), where the summer mean MDA8 ozone averaged across sites was 83 ppb in 2019 and the summer maximum MDA8 ozone averaged across sites was 129 ppb. In comparison, the Chinese air quality standard for annual maximum MDA8 ozone is 82 ppb. Mean summer MDA8 ozone increased by 3.3 ppb a^{-1} ($p<0.01$) in the NCP over the 2013–2019 period, which we attribute as 1.4 ppb a^{-1} ($p=0.02$) meteorologically driven and 1.9 ppb a^{-1} ($p<0.01$) anthropogenically driven.

Further investigation of the NCP trends shows that hot weather in June-July 2018–2019 was a major driver for the high ozone concentrations in those summers. Such hot weather does not relate to long-term warming but to interannual variability driven principally by foehn northwesterly winds. Removing this meteorological variability shows a sustained anthropogenic ozone increase over the NCP over the 2013–2019 record and persisting into 2018–2019. Examination of

ozone-relevant anthropogenic variables from the MEE network and from satellites shows a 49% decrease in $PM_{2.5}$ for 2013–2019 (15% for 2017–2019), a 25–30% decrease in NO_x emissions for 2013–2019 (6–10% for 2017–2019) and flat VOC emissions. The sustained anthropogenic increase in ozone over the 2017–2019 period may be explained by the continued decrease of $PM_{2.5}$, which scavenges the radical precursors of ozone, combined with flat emissions of VOCs. Reducing VOC emissions should be the top priority for reversing the increase of ozone in the NCP and in other urban areas of China.

Data availability. Hourly surface concentrations of air pollutants are archived at http://beijingair.sinaapp.com (last access: 30 June 2020). The MERRA-2 reanalysis data are from https://gmao.gsfc.nasa.gov/reanalysis/MERRA-2 (last access: 28 February 2020). The L3 OMI satellite data for NO_2 and HCHO are available at http://www.qa4ecv.eu/ecvs (last access: 28 February 2020). The L2 TROPOMI data for HCHO are available at https://s5phub.copernicus.eu/dhus (last access: 28 February 2020). The data used in this study can be accessed via doi (https://doi.org/10.7910/DVN/T6D7YY).

Author contributions. KL and DJJ designed the study. KL performed the analysis. LS and IDS provided the TROPOMI data. XL and HL contributed to the interpretation of the results. KL and DJJ wrote the paper with contributions from all co-authors

Competing interests. The authors declare that they have no conflict of interest.

Acknowledgements. This work is a contribution from the Harvard-NUIST Joint Laboratory for Air Quality and Climate. HL is supported by the National Natural Science Foundation of China (91744311). We appreciate the efforts from the China Ministry of Ecology and Environment for supporting the nationwide observation network and publishing hourly air pollutant concentrations. We acknowledge the QA4ECV project for the NO_2 and HCHO data. We appreciate the efforts from NASA GMAO for providing the MERRA-2 reanalysis data.

References

Boersma, K. F., Eskes, H. J., Richter, A., De Smedt, I., Lorente, A., Beirle, S., van Geffen, J. H. G. M., Zara, M., Peters, E., Van Roozendael, M., Wagner, T., Maasakkers, J. D., van der A, R. J., Nightingale, J., De Rudder, A., Irie, H., Pinardi, G., Lambert, J.-C., and Compernolle, S. C.: Improving Algorithms and Uncertainty Estimates for Satellite NO2 retrievals: Results from the Quality Assurance for the Essential Climate Variables (QA4ECV) Project, Atmos. Meas. Tech., 11, 6651-6678, http://dx.doi.org/10.5194/amt-11-6651-2018, 2018.

Chinese State Council: Action Plan on Air Pollution Prevention and Control (in Chinese), available at: http://www.gov.cn/zwgk/2013-09/12/content_2486773.htm (last access: 28 February 2020), 2013.

Chinese State Council: Three-Year Action Plan on Defending the Blue Sky (in Chinese), available at: http://www.gov.cn/zhengce/content/2018-07/03/content_5303158.htm (last access: 28 February 2020), 2018

Chen, R. and Lu, R.: Role of Large-Scale Circulation and Terrain in Causing Extreme Heat in Western North China, J. Clim., 29, 2511-2527, http://dx.doi.org/10.1175/jcli-d-15-0254.1, 2016.

Chen, Z., Chen, D., Kwan, M.-P., Chen, B., Gao, B., Zhuang, Y., Li, R., and Xu, B.: The control of anthropogenic emissions contributed to 80 % of the decrease in PM2.5 concentrations in Beijing from 2013 to 2017, Atmos. Chem. Phys., 19, 13519–13533, https://doi.org/10.5194/acp-19-13519-2019, 2019.

Dang, R. and Liao, H.: Radiative Forcing and Health Impact of Aerosols and Ozone in China as the Consequence of Clean Air Actions over 2012–2017, Geophys. Res. Lett., 46, 12511-12519, https://doi.org/10.1029/2019GL084605, 2019.

De Smedt, I., Stavrakou, T., Hendrick, F., Danckaert, T., Vlemmix, T., Pinardi, G., Theys, N., Lerot, C., Gielen, C., Vigouroux, C., Hermans, C., Fayt, C., Veefkind, P., Müller, J. F., and Van Roozendael, M.: Diurnal, Seasonal and Long-Term Variations of Global Formaldehyde Columns Inferred from Combined Omi and Gome-2 Observations, Atmos. Chem. Phys., 15, 12519-12545, http://dx.doi.org/10.5194/acp-15-12519-2015, 2015.

De Smedt, I., Theys, N., Yu, H., Danckaert, T., Lerot, C., Compernolle, S., Van Roozendael, M., Richter, A., Hilboll, A., Peters, E., Pedergnana, M., Loyola, D., Beirle, S., Wagner, T., Eskes, H., van Geffen, J., Boersma, K. F., and Veefkind, P.: Algorithm Theoretical Baseline for Formaldehyde Retrievals from S5p Tropomi and from the QA4ECV Project, Atmos. Meas. Tech., 11, 2395-2426, http://dx.doi.org/10.5194/amt-11-2395-2018, 2018.

Ding, D., Xing, J., Wang, S., Chang, X., and Hao, J.: Impacts of Emissions and Meteorological Changes on China's Ozone Pollution in the Warm Seasons of 2013 and 2017, Front. Environ. Sci. Eng., 13, 76, http://dx.doi.org/10.1007/s11783-019-1160-1, 2019.

Fan, H., Zhao, C., and Yang, Y.: A Comprehensive Analysis of the Spatio-Temporal Variation of Urban Air Pollution in China During 2014–2018, Atmos. Environ., 220, 117066, http://dx.doi.org/10.1016/j.atmosenv.2019.117066, 2020.

Fu, Y. and Tai, A. P. K.: Impact of climate and land cover changes on tropospheric ozone air quality and public health in East Asia between 1980 and 2010, Atmos. Chem. Phys., 15, 10093–10106, doi:10.5194/acp-15-10093-2015, 2015.

Fu, Y., Liao, H., and Yang, Y.: Interannual and Decadal Changes in Tropospheric oOzone in China and the Associated Chemistry-Climate Interactions: A Review, Adv. Atmos. Sci., 36, 975-993, https://doi.org/10.1007/s00376-019-8216-9, 2019

Gelaro, R., McCarty, W., Suarez, M. J., Todling, R., Molod, A., Takacs, L., Randles, C., Darmenov, A., Bosilovich, M. G., Reichle, R., Wargan, K., Coy, L., Cullather, R., Draper, C., Akella, S., Buchard, V., Conaty, A., da Silva, A., Gu,

W., Kim, G. K., Koster, R., Lucchesi, R., Merkova, D., Nielsen, J. E., Partyka, G., Pawson, S., Putman, W., Rienecker, M., Schubert, S. D., Sienkiewicz, M., and Zhao, B.: The Modern-Era Retrospective Analysis for Research and Applications, Version 2 (MERRA-2), J. Clim., 30, 5419-5454, http://dx.doi.org/10.1175/JCLI-D-16-0758.1, 2017.

Gong, C. and Liao, H.: A Typical Weather Pattern for Ozone Pollution Events in North China, Atmos. Chem. Phys., 19, 13725-13740, http://dx.doi.org/10.5194/acp-19-13725-2019, 2019.

Guenther, A. B., Jiang, X., Heald, C. L., Sakulyanontvittaya, T., Duhl, T., Emmons, L. K., and Wang, X.: The Model of Emissions of Gases and Aerosols from Nature version 2.1 (MEGAN2.1): an extended and updated framework for modeling biogenic emissions, Geosci. Model Dev., 5, 1471–1492, https://doi.org/10.5194/gmd-5-1471-2012, 2012.

Han, H., Liu, J., Shu, L., Wang, T., and Yuan, H.: Local and Synoptic Meteorological Influences on Daily Variability in Summertime Surface Ozone in Eastern China, Atmos. Chem. Phys., 20, 203-222, http://dx.doi.org/10.5194/acp-20-203-2020, 2020.

Jacob, D. J. and Winner, D. A.: Effect of Climate Change on Air Quality, Atmos. Environ., 43, 51-63, http://dx.doi.org/10.1016/j.atmosenv.2008.09.051, 2009.

Li, G., Bei, N., Cao, J., Wu, J., Long, X., Feng, T., Dai, W., Liu, S., Zhang, Q., and Tie, X.: Widespread and Persistent Ozone Pollution in Eastern China During the Non-Winter Season of 2015: Observations and Source Attributions, Atmos. Chem. Phys., 17, 2759-2774, http://dx.doi.org/10.5194/acp-17-2759-2017, 2017.

Li, K., Jacob, D. J., Liao, H., Shen, L., Zhang, Q., and Bates, K. H.: Anthropogenic Drivers of 2013-2017 Trends in Summer Surface Ozone in China, Proc. Natl. Acad. Sci. U.S.A., 116, 422-427, http://dx.doi.org/10.1073/pnas.1812168116, 2019a.

Li, K., Jacob, D. J., Liao, H., Zhu, J., Shah, V., Shen, L., Bates, K. H., Zhang, Q., and Zhai, S.: A Two-Pollutant Strategy for Improving Ozone and Particulate Air Quality in China, Nat. Geosci., 12, 906-910, http://dx.doi.org/10.1038/s41561-019-0464-x, 2019b.

Liu, J., Wang, L., Li, M., Liao, Z., Sun, Y., Song, T., Gao, W., Wang, Y., Li, Y., Ji, D., Hu, B., Kerminen, V.-M., Wang, Y., and Kulmala, M.: Quantifying the Impact of Synoptic Circulation Patterns on Ozone Variability in Northern China from April to October 2013-2017, Atmos. Chem. Phys., 19, 14477-14492, http://dx.doi.org/10.5194/acp-19-14477-2019, 2019.

Liu, Y. and Wang, T.: Worsening urban ozone pollution in China from 2013 to 2017 – Part 1: The complex and varying roles of meteorology, Atmos. Chem. Phys., 20, 6305-6321, https://doi.org/10.5194/acp-20-6305-2020, 2020.

Lu, X., Hong, J., Zhang, L., Cooper, O. R., Schultz, M. G., Xu, X., Wang, T., Gao, M., Zhao, Y., and Zhang, Y.: Severe Surface Ozone Pollution in China: A Global Perspective, Environ. Sci. Technol. Lett., 5, 487-494, http://dx.doi.org/10.1021/acs.estlett.8b00366, 2018.

Lu, X., Zhang, L., and Shen, L.: Meteorology and Climate Influences on Tropospheric Ozone: A Review of Natural Sources, Chemistry, and Transport Patterns, Curr. Pollut. Rep., 5, 238-260, http://dx.doi.org/10.1007/s40726-019-00118-3, 2019.

Lu, X., Zhang, L., Wang, X., Gao, M., Li, K., Zhang, Y., Yue, X., and Zhang, Y.: Rapid Increases in Warm-Season Surface Ozone and Resulting Health Impact in China since 2013, Environ. Sci. Technol. Lett., http://dx.doi.org/10.1021/acs.estlett.0c00171, 2020.

Ma, J., Xu, X., Zhao, C., and Yan, P.: A Review of Atmospheric Chemistry Research in China: Photochemical Smog, Haze Pollution, and Gas-Aerosol Interactions, Adv. Atmos. Sci., 29, 1006-1026, http://dx.doi.org/10.1007/s00376-012-1188-7, 2012.

Ministry of Ecology and Environment (MEE): Revision of the Ambien air quality standards (GB 3095-2012) (in Chinese), available at: http://www.mee.gov.cn/xxgk2018/xxgk/xxgk01/201808/t20180815_629602.html (last access: 28 February 2020), 2018.

Otero, N., Sillmann, J., Mar, K. A., Rust, H. W., Solberg, S., Andersson, C., Engardt, M., Bergström, R., Bessagnet, B., Colette, A., Couvidat, F., Cuvelier, C., Tsyro, S., Fagerli, H., Schaap, M., Manders, A., Mircea, M., Briganti, G., Cappelletti, A., Adani, M., D'Isidoro, M., Pay, M.-T., Theobald, M., Vivanco, M. G., Wind, P., Ojha, N., Raffort, V., and Butler, T.: A multi-model comparison of meteorological drivers of surface ozone over Europe, Atmos. Chem. Phys., 18, 12269–12288, https://doi.org/10.5194/acp-18-12269-2018, 2018.

Palmer, P. I., Abbot, D. S., Fu, T.-M., Jacob, D. J., Chance, K., Kurosu, T. P., Guenther, A., Wiedinmyer, C., Stanton, J. C., Pilling, M. J., Pressley, S. N., Lamb, B., and Sumner, A. L.: Quantifying the Seasonal and Interannual Variability of North American Isoprene Emissions Using Satellite Observations of the Formaldehyde Column, J. Geophys. Res., 111, http://dx.doi.org/10.1029/2005jd006689, 2006.

Shah, V., Jacob, D. J., Li, K., Silvern, R. F., Zhai, S., Liu, M., Lin, J., and Zhang, Q.: Effect of Changing NOx Lifetime on the Seasonality and Long-Term Trends of Satellite-Observed Tropospheric NO2 Columns over China, Atmos. Chem. Phys., 20, 1483-1495, http://dx.doi.org/10.5194/acp-20-1483-2020, 2020.

Shen, L., Mickley, L. J., and Gilleland, E.: Impact of increasing heat waves on US ozone episodes in the 2050s: Results from a multimodel analysis using extreme value theory, Geophys. Res. Lett., 43, 4017-4025, http://dx.doi.org/10.1002/2016GL068432, 2016.

Shen, L., Jacob, D. J., Liu, X., Huang, G., Li, K., Liao, H., and Wang, T.: An Evaluation of the Ability of the Ozone Monitoring Instrument (OMI) to Observe Boundary Layer Ozone Pollution across China: Application to 2005–2017 Ozone Trends, Atmos. Chem. Phys., 19, 6551-6560, http://dx.doi.org/10.5194/acp-19-6551-2019, 2019a.

Shen, L., Jacob, D. J., Zhu, L., Zhang, Q., Zheng, B., Sulprizio, M. P., Li, K., De Smedt, I., González Abad, G., Cao, H., Fu, T. M., and Liao, H.: The 2005–2016 Trends of Formaldehyde Columns over China Observed by Satellites:

Increasing Anthropogenic Emissions of Volatile Organic Compounds and Decreasing Agricultural Fire Emissions, Geophys. Res. Lett., 46, 4468-4475, http://dx.doi.org/10.1029/2019gl082172, 2019b.

Tai, A. P. K., Mickley, L. J., and Jacob, D. J.: Correlations between fine particulate matter ($PM_{2.5}$) and meteorological variables in the United States: Implications for the sensitivity of $PM_{2.5}$ to climate change, Atmos. Environ., 44, 3976–3984, 2010.

Tan, Z., Lu, K., Jiang, M., Su, R., Wang, H., Lou, S., Fu, Q., Zhai, C., Tan, Q., Yue, D., Chen, D., Wang, Z., Xie, S., Zeng, L., and Zhang, Y.: Daytime Atmospheric Oxidation Capacity in Four Chinese Megacities During the Photochemically Polluted Season: A Case Study Based on Box Model Simulation, Atmos. Chem. Phys., 19, 3493-3513, http://dx.doi.org/10.5194/acp-19-3493-2019, 2019.

Wang, T., Xue, L., Brimblecombe, P., Lam, Y. F., Li, L., and Zhang, L.: Ozone Pollution in China: A Review of Concentrations, Meteorological Influences, Chemical Precursors, and Effects, Sci. Total. Environ., 575, 1582-1596, http://dx.doi.org/10.1016/j.scitotenv.2016.10.081, 2017.

Wang, T., Dai, J., Lam, K. S., Nan Poon, C., and Brasseur, G. P.: Twenty-Five Years of Lower Tropospheric Ozone Observations in Tropical East Asia: The Influence of Emissions and Weather Patterns, Geophys. Res. Lett., 46, 11463-11470, https://doi.org/10.1029/2019GL084459, 2019

Yu, Y., Wang, Z., He, T., Meng, X., Xie, S., and Yu, H.: Driving Factors of the Significant Increase in Surface Ozone in the Yangtze River Delta, China, During 2013–2017, Atmos. Pollut. Res., 10, 1357-1364, http://dx.doi.org/10.1016/j.apr.2019.03.010, 2019.

Zhai, S., Jacob, D. J., Wang, X., Shen, L., Li, K., Zhang, Y., Gui, K., Zhao, T., and Liao, H.: Fine Particulate Matter (PM2.5) Trends in China, 2013–2018: Separating Contributions from Anthropogenic Emissions and Meteorology, Atmos. Chem. Phys., 19, 11031-11041, http://dx.doi.org/10.5194/acp-19-11031-2019, 2019.

Zhang, J., Wang, C., Qu, K., Ding, J., Shang, Y., Liu, H., and Wei, M.: Characteristics of Ozone Pollution, Regional Distribution and Causes During 2014–2018 in Shandong Province, East China, Atmosphere, 10, http://dx.doi.org/10.3390/atmos10090501, 2019.

Zhang, Q., Zheng, Y., Tong, D., Shao, M., Wang, S., Zhang, Y., Xu, X., Wang, J., He, H., Liu, W., Ding, Y., Lei, Y., Li, J., Wang, Z., Zhang, X., Wang, Y., Cheng, J., Liu, Y., Shi, Q., Yan, L., Geng, G., Hong, C., Li, M., Liu, F., Zheng, B., Cao, J., Ding, A., Gao, J., Fu, Q., Huo, J., Liu, B., Liu, Z., Yang, F., He, K., and Hao, J.: Drivers of Improved PM2.5 Air Quality in China from 2013 to 2017, Proc. Natl. Acad. Sci. U.S.A., 116, 24463-24469, http://dx.doi.org/10.1073/pnas.1907956116, 2019.

Zhang, X., Xu, X., Ding, Y., Liu, Y., Zhang, H., Wang, Y., and Zhong, J.: The impact of meteorological changes from 2013 to 2017 on PM2.5 mass reduction in key regions in China, Sci. China Earth Sci., 62, 1885–1902, https://doi.org/10.1007/s11430-019-9343-3, 2019.

Zheng, B., Tong, D., Li, M., Liu, F., Hong, C., Geng, G., Li, H., Li, X., Peng, L., Qi, J., Yan, L., Zhang, Y., Zhao, H., Zheng, Y., He, K., and Zhang, Q.: Trends in China's Anthropogenic Emissions since 2010 as the Consequence of Clean Air Actions, Atmos. Chem. Phys., 18, 14095-14111, http://dx.doi.org/10.5194/acp-18-14095-2018, 2018.

Zhu, L., Mickley, L. J., Jacob, D. J., Marais, E. A., Sheng, J., Hu, L., González Abad, G., and Chance, K.: Long-term (2005-2014) trends in formaldehyde (HCHO) columns across North America as seen by the OMI satellite instrument: Evidence of changing emissions of volatile organic compounds. Geophys. Res. Lett., 44, 7079–7086, http://dx.doi.org/10.1002/2017GL073859, 2017.

Table and Figure captions

Table 1. MDA8 ozone trends in China (ppb a^{-1}), 2013–2019 and 2013–2017.

Figure 1. Summer (JJA) concentrations of maximum MDA8 ozone (**a**), mean MDA8 ozone (**b**), maximum $PM_{2.5}$ (**c**), and mean $PM_{2.5}$ (**d**) for 2013–2019 at the network operated by the China Ministry of Ecology and Environment (MEE). Rectangles denote the four megacity clusters discussed in the text: North China Plain (NCP; 34°–41°N, 113°–119°E), Yangtze River Delta (YRD, 30°–33°N, 119°–122°E), Pearl River Delta (PRD, 21.5°–24°N, 112°–115.5°E), and Sichuan Basin (SCB, 28.5°–31.5°N, 103.5°–107°E).

Figure 2. Summertime ozone trends in China, 2013–2019. The left panel (**a**) shows observed trends of summer mean MDA8 ozone at MEE sites averaged on the 0.5° × 0.625° (≈50 × 50 km^2) MERRA-2 grid. The trends are obtained by ordinary linear regression and include sites with partial records. The middle panel (**b**) shows meteorologically driven trends determined by fitting ozone to meteorological covariates in the multiple linear regression (MLR) model. The right panel (**c**) shows anthropogenic trends as inferred from the residual of the MLR model. Statistically significant trends above the 90% confidence level are marked with black dots. The mean trends for all of China and for the four megacity clusters (rectangles) are inset, where the regression is applied to the spatially averaged MDA8 ozone for the cluster. Numbers in bold are statistically significant above the 90% confidence level (Table 1).

Figure 3. Summer mean trends of 850 hPa wind vectors (m s^{-1} a^{-1}) and surface daily maximum temperature (°C a^{-1}, shaded) over the period 2013–2019. Data are from the MERRA-2 reanalysis. The trends are obtained by ordinary linear regression of mean JJA data for individual years.

Figure 4. Time series of JJA daily maximum surface air temperatures over the North China Plain (NCP) for 1980–2019. Values are monthly means from the MERRA-2 reanalysis. The 2013–2019 period for the ozone trend analysis is shaded in grey.

Figure 5. June mean trends in meteorological variables over 2013–2019 under foehn (top) and non-foehn (bottom) conditions (**a**) Trends in 850 hPa winds (m s^{-1} a^{-1}) and surface daily maximum temperature (°C a^{-1}, shaded) under foehn conditions; (**b**) Trends in 500 hPa winds (m s^{-1} a^{-1}) and surface relative humidity (% a^{-1}, shaded) under foehn conditions; (**c**, **d**) are the same as (**a**, **b**) but for non-foehn conditions. Data are from the MERRA-2 re-analysis and trends are obtained by ordinary linear regression. Foehn conditions are diagnosed by a foehn index defined by the 850 hPa northwesterly wind averaged along a section from (42°N, 108°E) to (38°N, 112°E) (green line in **a**). The days with positive (negative) foehn index are taken as foehn (no-foehn) conditions. Meteorological data are from the MERRA-2 reanalysis.

Figure 6. Trends in summertime ozone and related anthropogenic drivers in the North China Plain (NCP). The left panel (**a**) shows time series of monthly mean MDA8 ozone (ppb) anomalies averaged over the MEE sites relative to the 2013–2019 summer (JJA) mean. Values are shown as anomalies for individual JJA months (3 points per year). Observed trends are compared to the meteorologically driven trends diagnosed by the MLR model, and to the residuals determining the anthropogenically driven trend. The right panel (**b**) shows time series of observed JJA mean quantities averaged over the NCP: $PM_{2.5}$ and NO_2 concentrations from the MEE sites, tropospheric NO_2 and HCHO column densities from the OMI satellite instrument, and HCHO column density from the TROPOMI satellite instrument. Values are presented as ratios relative to 2013. The TROPOMI HCHO data for 2018 have been scaled to the OMI data for that year with the multiplicative factor indicated in legend.

Table 1. MDA8 ozone trends in China (ppb a^{-1}), 2013–2019 and 2013–2017.

	JJA 2013–2019 trends			JJA 2013–2017 trends		
Regions	Observed[a]	Meteorological[b]	Anthropogenic[c]	Observed	Meteorological	Anthropogenic
China	**1.9** (*<0.01*)[d]	**0.7** (*<0.01*)	**1.2** (*<0.01*)	**1.7** (*<0.01*)	0.4 (*0.22*)	**1.3** (*<0.01*)
NCP	**3.3** (*<0.01*)	**1.4** (*0.02*)	**1.9** (*<0.01*)	**2.7** (*0.01*)	0.7 (*0.43*)	**2.0** (*<0.01*)
YRD	**1.6** (*<0.01*)	0.7 (*0.12*)	**0.9** (*<0.01*)	**1.7** (*0.03*)	0.2 (*0.82*)	**1.5** (*<0.01*)
PRD	**1.1** (*0.03*)	**0.8** (*0.07*)	0.3 (*0.29*)	0.6 (*0.44*)	0.4 (*0.65*)	0.3 (*0.51*)
SCB	0.7 (*0.23*)	-0.2 (*0.59*)	**1.0** (*<0.01*)	0.9 (*0.42*)	0.1 (*0.90*)	0.8 (*0.20*)

[a]Observed trends (OBS) are obtained by ordinary linear regression on summer (JJA) mean values of maximum daily 8-h average (MDA8) ozone measured at the sites of the Ministry of Ecology and Environment (MEE) network. The MDA8 ozone data are first averaged spatially over the 0.5° × 0.625° MERRA-2 grid (Figure 2), and then averaged nationally (China) and over four megacity clusters: North China Plan (NCP), Yangtze River Delta (YRD), Pearl River Delta (PRD), Sichuan Basin (SCB).

[b]Meteorologically-driven trends are obtained by fitting the ozone data to a multiple linear regression (MLR) model with the three most important meteorological covariates (see text).

[c]The anthropogenically-driven trends are obtained by ordinary linear regression of the residual ozone after removing the MLR-fitted value.

[d]p-values for the trends are in italics; trends in bold are those with p-value smaller than 0.1.

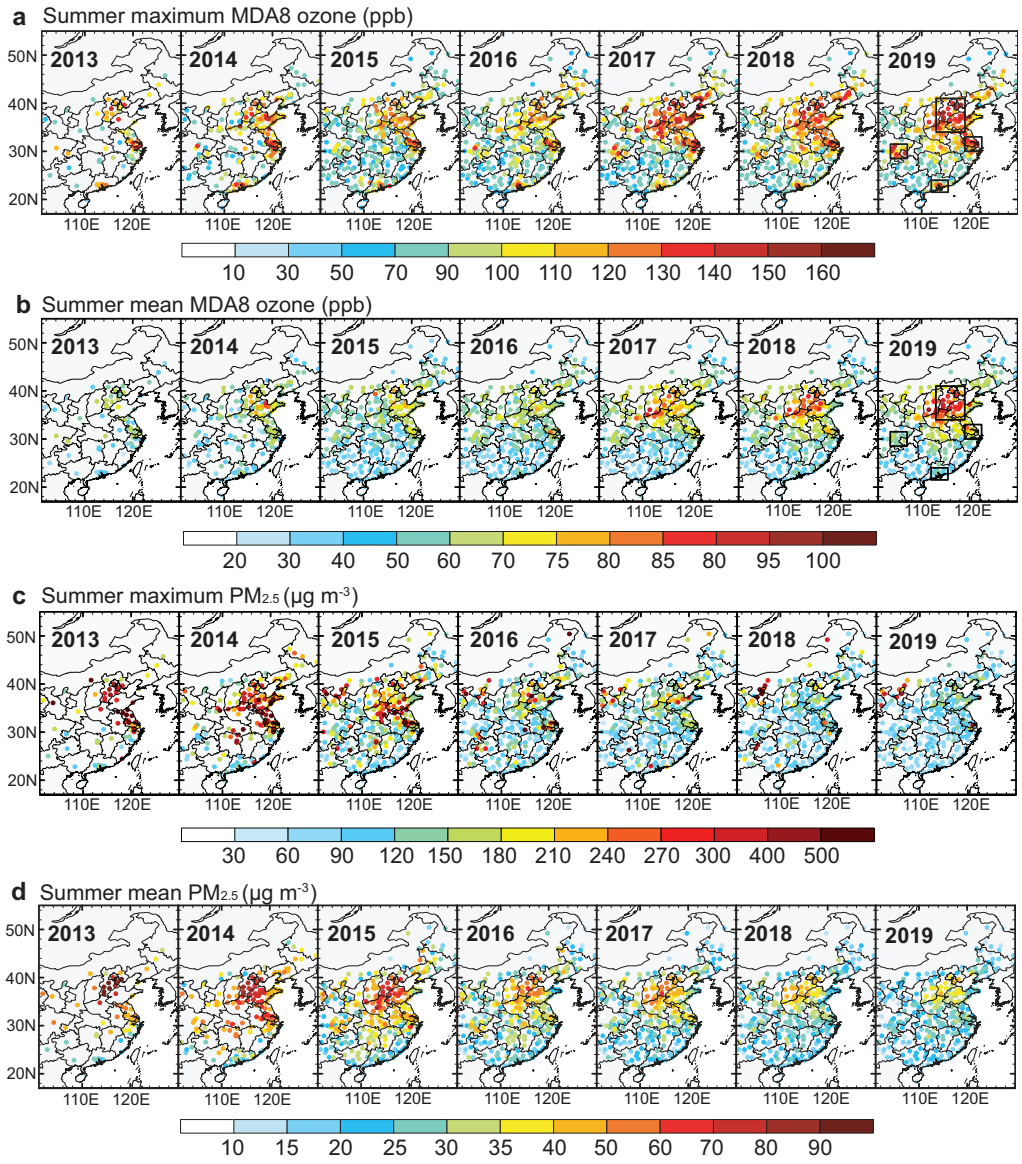

Figure 1. Summer (JJA) concentrations of maximum MDA8 ozone (**a**), mean MDA8 ozone (**b**), maximum $PM_{2.5}$ (**c**), and mean $PM_{2.5}$ (**d**) for 2013–2019 at the network operated by the China Ministry of Ecology and Environment (MEE). Rectangles denote the four megacity clusters discussed in the text: North China Plain (NCP; 34°–41°N, 113°–119°E), Yangtze River Delta (YRD, 30°–33°N, 119°–122°E), Pearl River Delta (PRD, 21.5°–24°N, 112°–115.5°E), and Sichuan Basin (SCB, 28.5°–31.5°N, 103.5°–107°E).

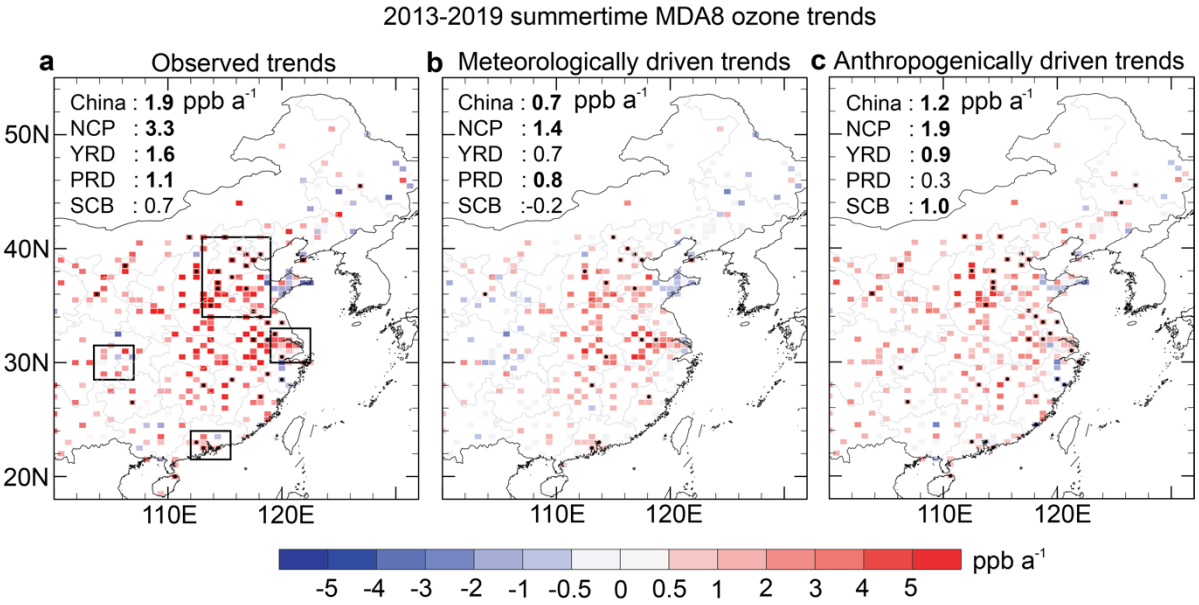

Figure 2. Summertime ozone trends in China, 2013–2019. The left panel (**a**) shows observed trends of summer mean MDA8 ozone at MEE sites averaged on the 0.5° × 0.625° (≈50 × 50 km^2) MERRA-2 grid. The trends are obtained by ordinary linear regression and include sites with partial records. The middle panel (**b**) shows meteorologically driven trends determined by fitting ozone to meteorological covariates in the multiple linear regression (MLR) model. The right panel (**c**) shows anthropogenic trends as inferred from the residual of the MLR model. Statistically significant trends above the 90% confidence level are marked with black dots. The mean trends for all of China and for the four megacity clusters (rectangles) are inset, where the regression is applied to the spatially averaged MDA8 ozone for the cluster. Numbers in bold are statistically significant above the 90% confidence level (Table 1).

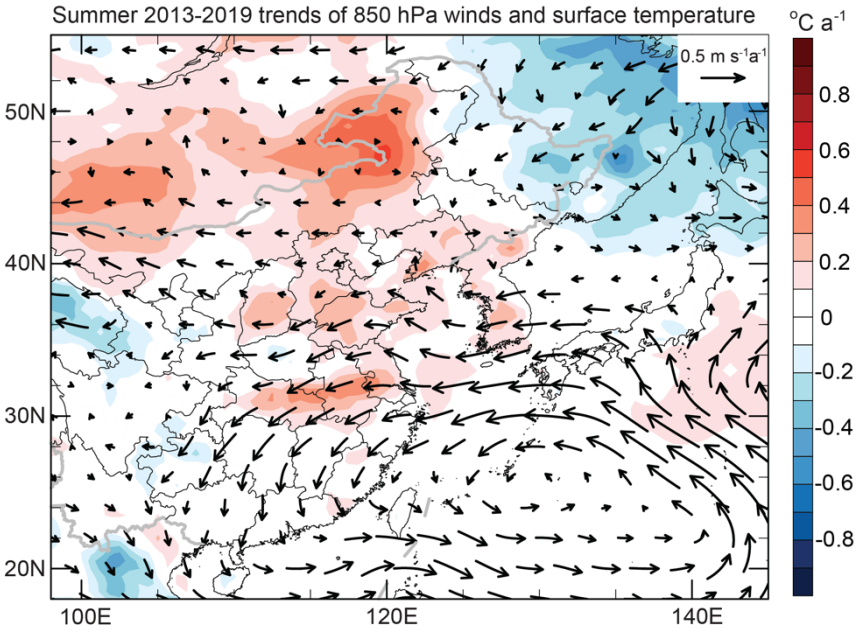

Figure 3. Summer mean trends of 850 hPa wind vectors (m s^{-1} a^{-1}) and surface daily maximum temperature (°C a^{-1}, shaded) over the period 2013–2019. Data are from the MERRA-2 reanalysis. The trends are obtained by ordinary linear regression of mean JJA data for individual years.

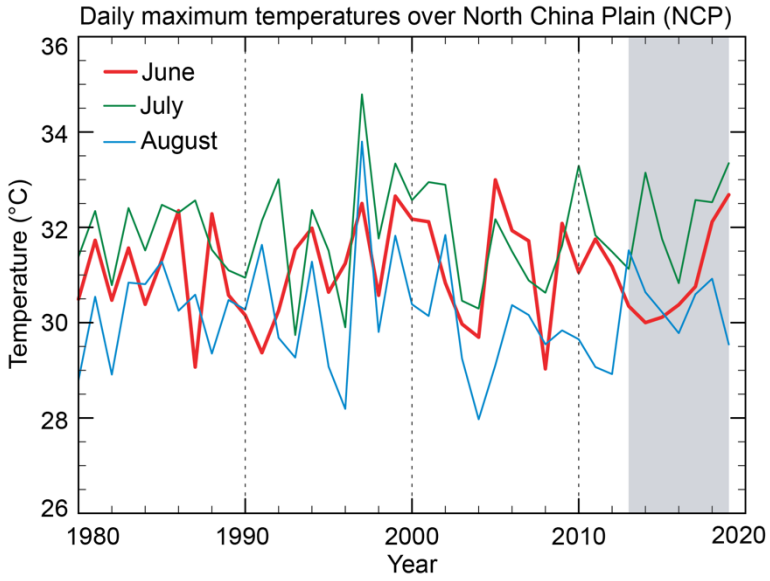

Figure 4. Time series of JJA daily maximum surface air temperatures over the North China Plain (NCP) for 1980–2019. Values are monthly means from the MERRA-2 reanalysis. The 2013–2019 period for the ozone trend analysis is shaded in grey.

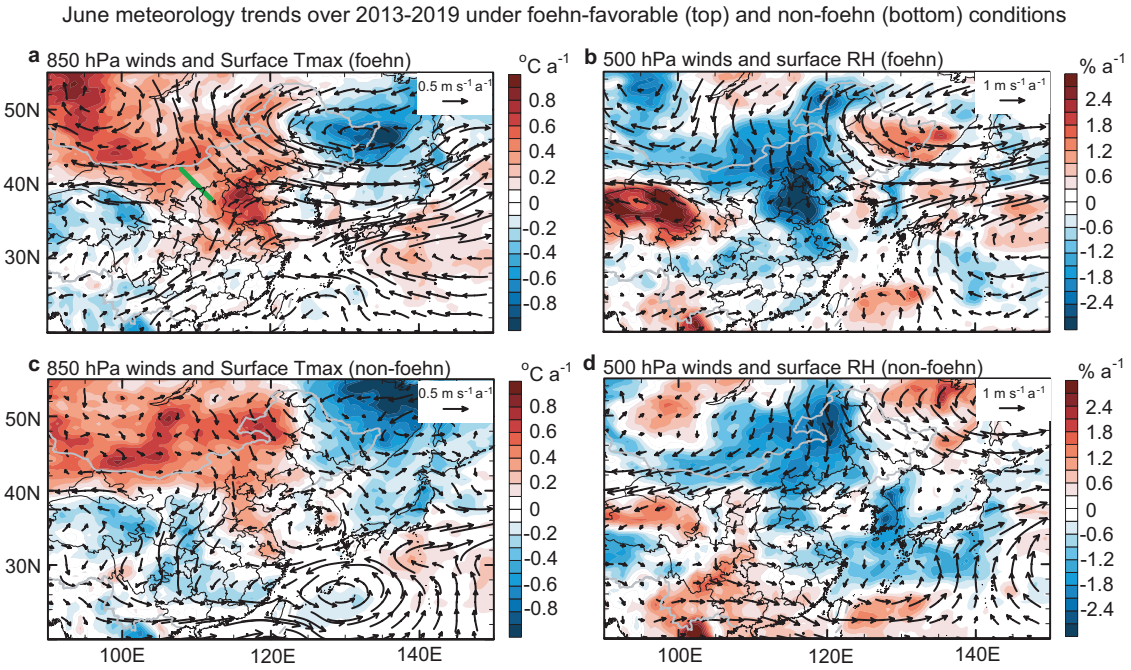

Figure 5. June mean trends in meteorological variables over 2013–2019 under foehn (top) and non-foehn (bottom) conditions (**a**) Trends in 850 hPa winds (m s^{-1} a^{-1}) and surface daily maximum temperature (°C a^{-1}, shaded) under foehn conditions; (**b**) Trends in 500 hPa winds (m s^{-1} a^{-1}) and surface relative humidity (% a^{-1}, shaded) under foehn conditions; (**c**, **d**) are the same as (**a**, **b**) but for non-foehn conditions. Data are from the MERRA-2 re-analysis and trends are obtained by ordinary linear regression. Foehn conditions are diagnosed by a foehn index defined by the 850 hPa northwesterly wind averaged along a section from (42°N, 108°E) to (38°N, 112°E) (green line in **a**). The days with positive (negative) foehn index are taken as foehn (no-foehn) conditions. Meteorological data are from the MERRA-2 reanalysis.

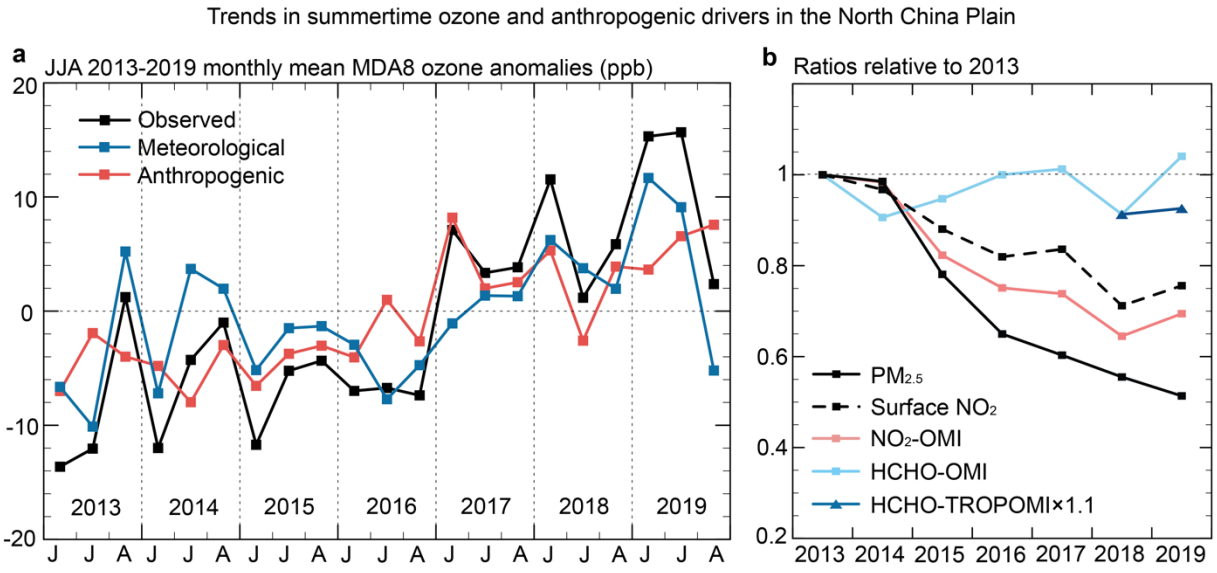

Figure 6. Trends in summertime ozone and related anthropogenic drivers in the North China Plain (NCP). The left panel (**a**) shows time series of monthly mean MDA8 ozone (ppb) anomalies averaged over the MEE sites relative to the 2013–2019 summer (JJA) mean. Values are shown as anomalies for individual JJA months (3 points per year). Observed trends are compared to the meteorologically driven trends diagnosed by the MLR model, and to the residuals determining the anthropogenically driven trend. The right panel (**b**) shows time series of observed JJA mean quantities averaged over the NCP: $PM_{2.5}$ and NO_2 concentrations from the MEE sites, tropospheric NO_2 and HCHO column densities from the OMI satellite instrument, and HCHO column density from the TROPOMI satellite instrument. Values are presented as ratios relative to 2013. The TROPOMI HCHO data for 2018 have been scaled to the OMI data for that year with the multiplicative factor indicated in legend.